Research Article

Cancer Immunology Research

The Combined Effect of FGFR Inhibition and PD-1 Blockade Promotes Tumor-Intrinsic Induction of Antitumor Immunity

Sangeetha Palakurthi[1], Mari Kuraguchi[1], Sima J. Zacharek[1], Enrique Zudaire[2], Wei Huang[1], Dennis M. Bonal[3], Jeffrey Liu[1], Abha Dhaneshwar[1], Kristin DePeaux[1], Martha R. Gowaski[1], Dyane Bailey[1], Samuel N. Regan[1], Elena Ivanova[1], Catherine Ferrante[2], Jessie M. English[1], Aditya Khosla[4], Andrew H. Beck[4], Julie A. Rytlewski[5], Catherine Sanders[5], Sylvie Laquerre[2], Mark A. Bittinger[1], Paul T. Kirschmeier[1], Kathryn Packman[2], Pasi A. Janne[1,6], Christopher Moy[2], Kwok-Kin Wong[1,7], Raluca I. Verona[2], and Matthew V. Lorenzi[2]

Abstract

The success of targeted or immune therapies is often hampered by the emergence of resistance and/or clinical benefit in only a subset of patients. We hypothesized that combining targeted therapy with immune modulation would show enhanced antitumor responses. Here, we explored the combination potential of erdafitinib, a fibroblast growth factor receptor (FGFR) inhibitor under clinical development, with PD-1 blockade in an autochthonous $FGFR2^{K660N}/p53^{mut}$ lung cancer mouse model. Erdafitinib monotherapy treatment resulted in substantial tumor control but no significant survival benefit. Although anti–PD-1 alone was ineffective, the erdafitinib and anti–PD-1 combination induced significant tumor regression and improved survival. For both erdafitinib monotherapy and combination treatments, tumor control was accompanied by tumor-intrinsic, FGFR pathway inhibition, increased T-cell infiltration, decreased regulatory T cells, and downregulation of PD-L1 expression on tumor cells. These effects were not observed in a $KRAS^{G12C}$-mutant genetically engineered mouse model, which is insensitive to FGFR inhibition, indicating that the immune changes mediated by erdafitinib may be initiated as a consequence of tumor cell killing. A decreased fraction of tumor-associated macrophages also occurred but only in combination-treated tumors. Treatment with erdafitinib decreased T-cell receptor (TCR) clonality, reflecting a broadening of the TCR repertoire induced by tumor cell death, whereas combination with anti–PD-1 led to increased TCR clonality, suggesting a more focused antitumor T-cell response. Our results showed that the combination of erdafitinib and anti–PD-1 drives expansion of T-cell clones and immunologic changes in the tumor microenvironment to support enhanced antitumor immunity and survival.

Introduction

Non–small cell lung cancer (NSCLC) is the leading cause of cancer-related mortality globally (1). Targeted agents directed at actionable mutated driver pathways such as EGFR, ALK, or ROS are the standard of care for subsets of NSCLC patients harboring these oncogenic alterations. Although targeted therapies have dramatically benefited patient care, invariably acquired resistance mutations or compensatory pathways are activated that neutralize the effectiveness of these therapies and limit the duration of clinical benefit. Patients progressing on targeted therapy have limited options, underscoring the significant unmet need to improve the durability of targeted therapy.

The fibroblast growth factor receptor (FGFR) family of receptor tyrosine kinases is composed of four members (FGFR1–4) that mediate the function of the FGFR ligand family (2). Binding of FGF to FGFR induces receptor dimerization, resulting in transphosphorylation of the tyrosine kinase intracellular domain, leading to activation of downstream signaling cascades. FGFRs are critical mediators of a wide variety of functions, including embryonic development, cell proliferation, differentiation, angiogenesis, and migration (3). In cancer, FGFR function is often subverted by constitutive activation through gene amplification, point mutation, or chromosomal rearrangement in a variety of tumor types. FGFR activation by chromosomal rearrangement was first observed in osteosarcoma

[1]Belfer Center for Applied Cancer Science, Dana-Farber Cancer Institute, Boston, Massachusetts. [2]Janssen, Pharmaceutical Companies of Johnson & Johnson, Spring House, Pennsylvania. [3]Lurie Family Imaging Center, Dana-Farber Cancer Institute, Boston, Massachusetts. [4]PathAI, Boston, Massachusetts. [5]Adaptive Biotechnologies, Seattle, Washington. [6]Department of Medical Oncology, Dana-Farber Cancer Institute, Boston, Massachusetts. [7]Laura & Isaac Perlmutter Cancer Center, NYU Langone Medical Center, New York University, New York, New York.

Note: Supplementary data for this article are available at Cancer Immunology Research Online (http://cancerimmunolres.aacrjournals.org/).

S. Palakurthi, M. Kuraguchi, S. Zacharek, E. Zudaire, and R.I. Verona contributed equally to this article.

Current address for J.A. Rytlewski: Juno Therapeutics, Seattle, Washington.

Corresponding Authors: Raluca I. Verona, Janssen Research & Development, 1400 McKean Road, Spring House, PA 19477. Phone: 215-628-5211; E-mail: rverona@its.jnj.com; and Matthew V. Lorenzi, mlorenzi@its.jnj.com

Cancer Immunol Res 2019;7:1457–71

doi: 10.1158/2326-6066.CIR-18-0595

(4), and subsequent large-scale tumor sequencing initiatives revealed frequent dysregulation of the FGFR family in NSCLC and other tumor types (5, 6). Preclinical analysis of these genetic alterations in model systems has revealed these mutations to be potent oncogenes *in vitro* and *in vivo* (7, 8).

The high frequency of *FGFR* genetic alterations in human cancers provides a compelling rationale to advance specific FGFR inhibitors for patients with *FGFR* genetic aberrations. Erdafitinib is a selective pan-FGFR inhibitor that has demonstrated preclinically potent antitumor activity in patient-derived xenograft models driven by *FGFR* mutation (9). Erdafitinib is currently being examined in clinical studies in patients with *FGFR*-activating mutations and has demonstrated clinical benefit in bladder cancer patients with *FGFR* point mutations or gene rearrangements (10, 11). However, similar to other targeted agents, it is important to examine combination strategies that can prolong clinical benefit in patients with *FGFR* alterations.

Cancer immunotherapies, such as those targeting the immune checkpoint PD-1, have revolutionized cancer treatment across a variety of tumor types, including NSCLC. However, only a subset of patients benefits from PD-1/PD-L1 checkpoint blockade. Lack of response to immunotherapy is characterized by several factors, such as a noninflamed tumor microenvironment (TME) with limited infiltrating T cells and/or the presence of immunosuppressive cell types. Tumor genetics can also influence response to checkpoint inhibitors, as evidenced by reports showing that activation of the β-catenin/Wnt pathway renders a non-T cell–inflamed TME (12). Patients with tumors carrying low mutational burden or certain driver pathway mutations such as ALK or EGFR benefit much less from anti–PD-1 or anti–PD-L1 therapy due to a lack of an inflammatory microenvironment and $CD8^+$ T cells that recognize tumor neoantigens (13–15). Overall, these data suggest that defects in antitumor immunity need to be addressed to extend immunotherapy benefit in patients with these driver pathway mutations (16). Here, we specifically explored the contribution of tumor-intrinsic targeting of FGFR driver pathway mutations and its impact on remodeling the TME in an autochthonous lung cancer FGFR2-driven mouse model with low mutational burden (17). Our data showed the key role of FGFR inhibition on remodeling the immune microenvironment of tumors, especially inducing new T-cell responses, which in turn acts in concert with anti–PD-1 to promote antitumor immunity. These results provide a rationale for the combined clinical testing of erdafitinib and PD-1 blockade in patients with FGFR-altered tumors.

Materials and Methods

Genetically engineered mouse models

The FGFR2-mutant transgenic mouse strain conditionally expressing human FGFR2 with the kinase domain activating mutation [$Col1a1^{tm4(CAG\text{-}FGFR2\_iIIIb^*K660N)Kkw}$ ($FGFR2^{K660N}$), Kwok-Kin Wong Lab, New York, NY] and its compound strain, p53 conditional knockout mice [$Trp53^{tm1Brn}$ ($Trp53^{FL/FL}$), Jackson Laboratories, #8462], were previously described (7). For all studies, mice used were hemizygous for $FGFR2^{K660N}$ with the p53 inactivation mutation, either $Trp53^{R270H/+}$ (Jackson Laboratories, #8651) or $Trp53^{FL/FL}$, and on a mixed genetic background (C57BL/6, BALB/c, and 129S). Intratracheal instillation of Adeno-cre virus (5.0×10^7 pfu/mouse, University of Iowa, Iowa City, IA) was administered into the lungs by intratracheal instillation using a catheter when mice were 7 to 10 weeks of age as described previously (18). All mouse experiments were performed with the approval of the institutional animal care and use committee at Dana-Farber Cancer Institute (DFCI; Boston, MA).

The *KRAS*-mutant transgenic mouse strain conditionally expressing human *KRAS* with the $KRAS^{G12C}$ oncogenic mutation (19) was monitored for tumor development by MRI after intratracheal induction with Adeno-cre virus (1×10^6 pfu/mouse, University of Iowa) when mice were 7 to 10 weeks of age. Mice with lung tumors confirmed by MRI were randomized into four treatment groups for short-term pharmacodynamic studies as described in Materials and Methods.

Treatment studies

Mice with lung tumors confirmed by MRI were randomized into four treatment groups: control, anti–PD-1 (10 mg/kg, Bio X Cell, RMP1-14), erdafitinib [Janssen Pharmaceuticals, 12.5 mg/kg in 20% 2-hydroxypropyl-β-cyclodextrin (HPβCD), pH 4.0], and combination of erdafitinib and anti–PD-1. Control animals were treated with 20% HPβCD, pH 4.0, and rat IgG2A isotype (10 mg/kg, Bio X Cell, 2AS). For long-term survival study, mice were dosed intraperitoneally twice a week with anti–PD-1 or rat IgG2A isotype and orally twice a day with erdafitinib for 4 weeks. After treatment initiation, mice were imaged at weeks 2, 4, and 6 and monitored for survival endpoints for up to 30 weeks. For short-term pharmacodynamic studies, mice were dosed intraperitoneally every other day with either anti–PD-1 or rat IgG2A isotype and orally twice a day with erdafitinib for a week. Baseline blood samples were collected by retro-orbital bleeding, transferred into EDTA tubes (Thermo Fisher, #02-669-38CS), snap frozen, and stored at –80C. Treated mice were anesthetized with ketamine/xylazine at 80/10 mg per kg, perfused transcardially with 10 mL PBS, and harvested for tumors, lungs, and blood on day 8, 4 hours after the final dose of erdafitinib or 28 hours after the final dose of anti–PD-1 for immunohistochemistry (IHC), flow cytometry, and T-cell receptor (TCR) sequencing analyses. Lung tumor volumes were calculated from MRI images using the 3D Slicer software (http://www.slicer.org). Mice that did not survive the first MRI session after recruitment or those that died of causes other than lung carcinogenesis were excluded from the study, and only those that met the criteria were included for both efficacy and survival reads.

IHC

Mouse lungs were fixed in 10% buffered formalin overnight, transferred to 70% ethanol, and then embedded in paraffin. Formalin-fixed, paraffin-embedded (FFPE) sections (5 μm) were cut for hematoxylin and eosin (H&E) staining and also stained for IHC (Supplementary Table S1). Tumor regions were quantitated using Aperio Imaging System from images of tumor nodules stained for the indicated markers and averaged, with a minimum sample size of 5 animals per treatment group. Ten images were acquired for each mouse for analysis.

Patients with *KRAS*-mutant and *FGFR*-mutant NSCLC were identified through an institutional database of patients who had undergone genotyping as previously described (20, 21). The study was conducted in accordance with ethical standards of the Declaration of Helsinki. All 89 patients were consented to an institutional review board (IRB)–approved protocol allowing specimen collection and clinical data on a correlative

science study. Inclusion criteria specified that the patients needed to have a diagnosis of a thoracic malignancy and be receiving their treatment at DFCI. Only diagnostic tumor tissue was collected; tumor samples were fixed in formalin and embedded in paraffin according to standard laboratory pathology practice, and stored at the department of pathology at the Brigham and Women's Hospital (Boston, MA). FFPE tissue sections (4 μm) were stained for both PD-L1 and CD3 (Supplementary Table S1), and stained slides were digitally scanned using an Aperio XT instrument at 20× magnification. The whole tumor section was scanned on Aperio. PD-L1 staining was visually scored by a pathologist with the generation of the H-score: the percentage of area stained multiplied by the weighted intensity. CD3 quantification was performed by PathAI company (https://www.pathai.com/) on Aperio-scanned images.

Primary tissue dissociation and flow cytometry

Collected lungs were also submerged in PBS containing 5 mmol/L EDTA. Lung tissue was placed in gentleMACS C Tube (Miltenyi, #130-096-334) and dissociated in collagenase type IV (Worthington, #LS004186) and DNase I (Roche #10104159001)–containing Hank's Balanced Salt Solution (HBSS; Gibco, #24020117) plus 1× HEPES (Gibco, #15630080); tissues were dissociated using the gentleMACS Dissociator (Miltenyi) under program "lung_02." Samples were then incubated at 37°C for 30 minutes with gentle mixing on a rotator followed by a second dissociation using program "imptumor_01." The dissociated lung samples were passed through a 70-μm filter (Falcon) and rinsed with RPMI (Gibco, #72400) containing 10% FBS (HyClone, #SH300088.03). Dissociated cells were stained for viability with the Zombie Aqua Fixable Viability kit (BioLegend, #423102) according to the manufacturer's protocol. Fc receptors were blocked with TruStain fcX (BioLegend, #420301) on ice for 15 minutes, followed by staining for surface proteins (Supplementary Table S1). Cells were fixed and permeabilized using the Foxp3/Transcription Factor Staining Buffer Set (eBioscience, #00-5523-00) for intracellular staining (Supplementary Table S1). AccuCheck Counting Beads (Life Technologies, #PCB100) were added to each sample for cell number quantification. Samples were analyzed on a BD LSRFortessa X-20 equipped with FACSDiva software, and further data analysis was performed with FlowJo software (Tree Star). Markers and gating strategy for flow cytometry are shown in Supplementary Table S2.

TCRβ immunosequencing

Collected tissues (approximately 250 μL blood, or 10 mg fragment or 100k cells from dissociated tumor-bearing lung) were snap frozen and stored at –80C until analysis. Immunosequencing of the CDR3 regions of mouse TCRβ chains was performed using the immunoSEQ Assay (Adaptive Biotechnologies). Genomic DNA was extracted from cell suspensions using the DNAeasy Blood and Tissue Kit (Qiagen), from tissue using the QIAsymphony DSP DNA Mini Kit (Qiagen), and from blood using the QIASymphony DNA Midi Kit (Qiagen). DNA content was measured using the DropSense 96 Spectrophotometer. Extracted genomic DNA (up to 2.67 μg) was amplified in a bias-controlled multiplex PCR (Adaptive Biotechnologies), followed by high-throughput sequencing. Sequences were collapsed and filtered to identify and quantitate the absolute abundance of each unique TCRβ CDR3 region for further analysis as previously described (22–24). Data are available at https://clients.adaptivebiotech.com/pub/palakurthi-2019-cir.

Statistical analyses of *TCRB* immunosequencing data

Clonality was defined as 1- Peilou eveness (25) and was calculated on productive rearrangements by

$$\frac{1+\sum_{i}^{N} p_i \log_2(p_i)}{\log_2(N)}$$

where p_i is the proportional abundance of rearrangement i, and N is the total number of rearrangements. Clonality values range from 0 to 1 and describe the shape of the frequency distribution: Clonality values approaching 0 indicate a very even distribution of frequencies, whereas values approaching 1 indicate an increasingly asymmetric distribution in which a few clones are present at high frequencies. Clonality between experimental groups was compared using a two-tailed Wilcoxon rank sum test. Correlations between T-cell fraction or clonality and tumor size data were assessed using Spearman rank correlation after running a Shapiro–Wilk test for normality. Clonal expansion was quantified by differential abundance analysis of clone frequencies between two samples from the same individual, which uses a binomial test with an FDR of 1% as previously described (26). Hierarchical clustering of clones by frequency was performed using a Ward linkage with Euclidean distances. Statistical analyses were performed in R version 3.3.

Cell culture, *in vitro* studies, and Western blotting

The KATO III cell line was maintained in IMDM supplemented with 20% FBS, and the H441 cell line was grown in RPMI supplemented with 10% FBS. All cell lines were from ATCC. KATO III cells were cultured in the presence of 40 ng/mL human FGF-2 (Miltenyibiotec, #130-093-839) and human IFNγ (Thermo Fisher, #RIFNG100) at a concentration of 5 ng/mL.

For FACS analysis, a day after plating 25,000 cells per well in a 96-well plate, cells were treated with 0.01 to 500 nmol/L erdafitinib (or BGJ398 or AZD4547, Selleck Chemicals) for 24 hours, and then collected, pelleted, and resuspended in FACS buffer (PBS + 2% FBS). Cells were stained with anti-human CD274 (B7-H1, PD-L1; BioLegend, #329707) and Zombie Violet Viability Kit (BioLegend, #423113) and analyzed by flow cytometry as described above.

For Western blotting, 750,000 cells were plated per well in a six-well plate and 24 hours later, were treated with 0.1 to 500 nmol/L erdafitinib (or rapamycin, trametinib, ruxolitinib, or SH-4-54; Selleck Chemicals) for 1.5 hours. Cells were collected and lysed in RIPA lysis buffer (Boston BioProducts) with 0.5 M EDTA, 1 mmol/L dithiothreitol (DTT), 1 mmol/L phenylmethylsulfonyl fluoride (PMSF), and 1× Halt protease inhibitor cocktail (Thermo Fisher Scientific). Following rotation at 4°C for 20 minutes, lysates were cleared by centrifugation (16,000 × *g*) for 15 minutes. Cleared lysates were quantified using the Pierce BCA Protein Assay Kit (Thermo Fisher Scientific) according to the manufacturer's instructions. For each lysate, 30 μg of total protein was separated by SDS-PAGE (Bio-Rad, #4561085) and transferred to nitrocellulose (Thermo Fisher, IB23002). After blocking for 1 hour in 5% w/v bovine serum albumin (BSA) in Tris-buffered saline (TBS; 0.1% Tween 20) buffer, membranes

were stained for various proteins (Supplementary Table S1; antibodies diluted in 5% BSA in TBST at dilutions recommended per manufacturer) overnight at 4°C with gentle rocking. Blots were stained with Horse Radish Peroxidase–conjugated goat anti-rabbit or anti-mouse secondary antibody (Jackson ImmunoResearch Laboratories) at a 1/4,000 dilution in 5% BSA in TBST for 1 hour. Blots were incubated for 90 seconds in the SuperSignal West Pico or Femto Chemiluminescent Substrate Kit (Thermo Scientific, PG205923 or 34094, respectively), and staining was visualized using a FluorChem imaging system (ProteinSimple).

Analysis of FGFR2 mutation data across adenocarcinoma and squamous NSCLC

Mutation data were compiled from Genomics Evidence Neoplasia Information Exchange (GENIE; ref. 27; version 4.0) and The Cancer Genome Atlas (TCGA) cBioPortal (www.cbioportal.org) for lung squamous cell (6) and lung adenocarcinomas (28). Functional domain for FGFR2 was defined from Uniprot (https://www.uniprot.org/uniprot/P21802) entry for FGFR2 and annotated to indicate mutations that are located in the kinase domain between positions 441 and 770.

In vitro functional assays

Peripheral blood mononuclear cell viability assays. Peripheral blood mononuclear cells (PBMC) from healthy donors (Biological Specialty Corporation), plated at 200,000 cells/well, were either unstimulated or stimulated with 1 ng/mL anti-CD3 antibodies (clone OKT3, Janssen) for the duration of the experiment and were treated with increasing concentrations of erdafitinib (0.0000077, 0.000023, 0.000070, 0.00021, 0.00063, 0.00188, 0.00565, 0.01694, 0.051, 0.152, 0.457, 1.372, 4.115, 12.346, 37.037, 111.111, 333.333, and 1000 nmol/L). On days 2 and 6 after plating, cell viability was assessed by CellTiter-Glo (Promega). Reactions were run in triplicate.

Mixed lymphocyte reactions. Human $CD4^+$ T cells were isolated from PBMCs from healthy donors (Biological Specialty Corporation) using a $CD4^+$ isolation kit (Miltenyi Biotec, catalog #130-096-533). Purified human $CD4^+$ T cells (100,000) were activated by stimulation with 5,000 allogeneic, major histocompatibility complex-mismatched, dendritic cells (DC; Hemacare) for 5 days in the presence of anti-human PD-1 antibodies (nivolumab analogue antibody, Janssen) at 30, 10, 3.33, 1.11, 0.37, and 0.12 nmol/L (from left to right) or isotype control at 30 nmol/L (Janssen). Erdafitinib was added at 1,000, 500, or 100 nmol/L alone, with anti–PD-1 at concentrations indicated above or with isotype-control antibody (Janssen) at 30 nmol/L. Cell culture supernatants were analyzed for IFNγ levels [Meso Scale Discovery (MSD), catalog #K151AEB-2).

Cytomegalovirus recall assays. In the cytomegalovirus (CMV) recall assays, 150,000 PBMCs isolated from the peripheral blood of CMV-responsive donors (Astarte Biologics) were stimulated with 0.1 μg/mL CMV antigen (Astarte Biologics, catalog #1004) for 6 days in the presence of anti-human PD-1 (nivolumab analogue antibody, Janssen) at doses from left to right of 30, 10, 3.33, 1.11, 0.37, and 0.12 nmol/L. Erdafitinib was added at 1,000, 500, or 100 nmol/L alone or together with anti–PD-1 at concentrations indicated above or isotype-control antibody (Janssen) at 30 nmol/L. Cell culture supernatants were analyzed for IFNγ using the MSD kit. Cell culture supernatants were analyzed for IFNγ levels (MSD, catalog #K151AEB-2).

Statistical analysis

Tumor volume changes between treatment groups were compared using one-way ANOVA and Dunnett multiple comparisons test. *P* values for all survival curves were assessed by the log-rank Mantel–Cox test. *P* values for IHC and flow cytometry data were assessed by the Student *t* test with Welch correction (GraphPad Prism). *P* values for comparisons between responders and nonresponders were assessed by a two-tailed Wilcoxon rank sum test (GraphPad Prism).

Results

Antitumor response and improved survival with erdafitinib and anti–PD-1 combination

The efficacy of the pan-FGFR inhibitor erdafitinib, both as a single agent and in combination with anti–PD-1, was evaluated in Lox-Stop-Lox-$FGFR2^{K660N}$;$p53^{mut}$ (FKNP) mice, a fully immunocompetent genetically engineered mouse model (GEMM) of lung cancer driven by an inducible activating mutation in the kinase domain of *FGFR2* (7). FKNP mice develop lung adenocarcinomas with a latency of approximately 35 weeks after intratracheal delivery into lungs of adenovirus-expressing Cre recombinase. Mutations in *FGFR2*, including in the kinase domain, have been reported in both squamous and adenocarcinoma NSCLC based on mutation data compiled from the GENIE and TCGA data sets (Supplementary Table S3), highlighting the clinical relevance of this model. FGFR-altered human cancers have been previously correlated with a non-T cell–inflamed TME (29). To determine if FKNP tumors shared features of FGFR-driven human tumors, we used flow cytometry to evaluate the TME (Supplementary Fig. S1). We observed a significant decrease in T and natural killer (NK) cells relative to normal lung (Supplementary Fig. S1A–S1C) and an increase in $CD11c^+CD11b^-$ tumor-associated alveolar macrophages (TAM; ref. 30), regulatory T cells (Treg), and exhaustion marker–positive (PD-1, TIM-3, and LAG-3) T cells (Supplementary Fig. S1F and S1H–S1N). The fraction of PD-L1–positive tumor cells was increased relative to normal lung (Supplementary Fig. S1O). Together, these data suggest an immune-suppressive microenvironment in FKNP lung tumors.

MRI-confirmed lung tumor–bearing mice were randomized into four different treatment groups and treated for 4 weeks, followed by survival monitoring (Fig. 1A; Supplementary Fig. S2A). All treatments were well tolerated, with no significant loss in body weight during duration of treatment (Supplementary Fig. S2B). Treatment with anti–PD-1 alone did not reduce tumor burden at any time point after treatment. In contrast, partial or complete tumor regressions [average of 80% tumor growth inhibition (TGI)] were observed in all mice treated with erdafitinib monotherapy or in combination with anti–PD-1 at 2 to 4 weeks after treatment initiation and persisted until week 6, 2 weeks after treatment termination (Fig. 1B and C; $P = 0.0001$ at 2 and 4 weeks). No differences in TGI were observed between erdafitinib monotherapy and anti–PD-1 combination groups within the first 6 weeks of MRI monitoring (Fig. 1B and C). However, a significant survival advantage was observed in mice treated with the combination (19.7 weeks) compared with control (10.2 weeks; $P < 0.0005$) and erdafitinib (13.4 weeks; $P < 0.004$) groups (Fig. 1D).

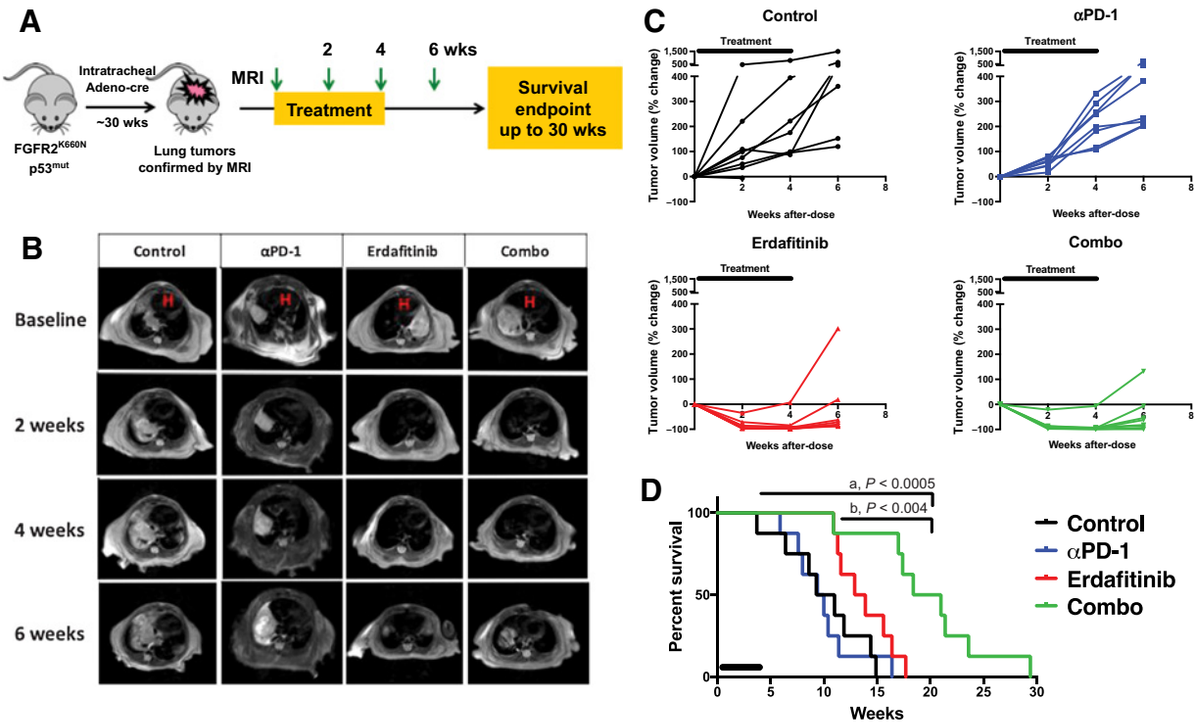

Figure 1.

Antitumor response and improved survival with erdafitinib and anti–PD-1 combination. **A,** Efficacy study design in FGFR2^{K660N};p53^{mut} (FKNP) lung tumor–bearing mice. Mice were treated with either control (vehicle + rat IgG2a isotype), anti–PD-1, erdafitinib, or erdafitinib + anti–PD-1, and were monitored for survival after 4 weeks of dosing (n = 8/group). wks, weeks. **B,** Representative serial MRIs of lung tumors in FKNP mice treated for 4 weeks. Images represent baseline and 2, 4, and 6 weeks after the start of treatment (red H, the heart). **C,** Percentage of tumor volume changes in each treatment group quantified from MRI using 3D Slicer software at baseline and 2, 4, and 6 weeks after the start of treatment. Solid black line represents the treatment duration. **D,** Kaplan–Meier survival curves across treatment groups in FKNP lung tumor–bearing mice, demonstrating significant survival benefit with combination over either control (a, $P < 0.0005$) or erdafitinib monotherapy (b, $P < 0.004$, log-rank test). Solid black line represents the treatment duration.

In contrast to the FKNP model, a KRAS-driven lung cancer GEMM was insensitive to erdafitinib alone or in combination with anti–PD-1 (Supplementary Fig. S3A and S3B; Supplementary Table S4), suggesting that the observed effects were mediated through FGFR blockade in the FKNP model.

Erdafitinib alone or in combination with anti–PD-1 suppresses FGFR signaling

We next performed a separate short-term pharmacodynamic study in FKNP mice using the dosing and tissue collection schedule shown in Fig. 2A. As with the previous study (Fig. 1), over 90% of animals showed significant tumor regressions, as assessed by MRI (Fig. 2B and C; Supplementary Fig. S3A; Supplementary Table S5) after 1 week of treatment with erdafitinib alone or in combination with anti–PD-1. Under these treatment conditions, we profiled treatment-induced changes in signaling and the TME by IHC and flow cytometry. FGFRs signal through a key intracellular binding partner, FGFR substrate 2 alpha (FRS2α), that leads to MAPK and PI3K/AKT pathway activation (31, 32). A significant decrease in phospho-FRS2α (Y436) was observed 8 days after treatment with erdafitinib alone or in combination with anti–PD-1 (Fig. 2D–F), and decreased levels of phospho-S6 (S235/236) were seen in all treatment groups when compared with isotype control (Fig. 2E–G). These results indicated that constitutive FGFR activity and downstream signaling were suppressed by erdafitinib in FKNP mice, which correlated with antitumor activity.

Effects on immune cell infiltration and proliferation

To examine the basis for anti–PD-1 and erdafitinib combination on antitumor activity, we profiled treatment-induced changes in tumor and immune cell subsets (Fig. 3; Supplementary Fig. S4A–S4O). Consistent with the inhibition of FGFR signaling and tumor growth in erdafitinib-treated groups, a significant global decrease in Ki67$^+$ proliferating cells was detected by IHC (Fig. 3A) compared with vehicle or anti–PD-1–treated animals. Evaluation by flow cytometry revealed that the proportion of proliferative epithelial cells (EpCAM$^+$Ki67$^+$) was reduced by erdafitinib therapy alone or in combination with anti–PD-1 (Fig. 3C). We also examined treatment effects on different immune cells in the TME by both IHC and flow cytometry and observed a significant increase in infiltrating T cells in erdafitinib-treated groups (Fig. 3B and 3D–G; Supplementary Fig. S4P). A reduction in CD3$^+$Ki67$^+$ T cells was induced by erdafitinib (Fig. 3E; Supplementary Fig. S4K and S4L), which was paralleled by increases in central memory and effector CD4$^+$ and CD8$^+$ T cells (Fig. 3H and I; Supplementary Fig. S4N and S4O). Infiltration of CD8$^+$ T cells was correlated

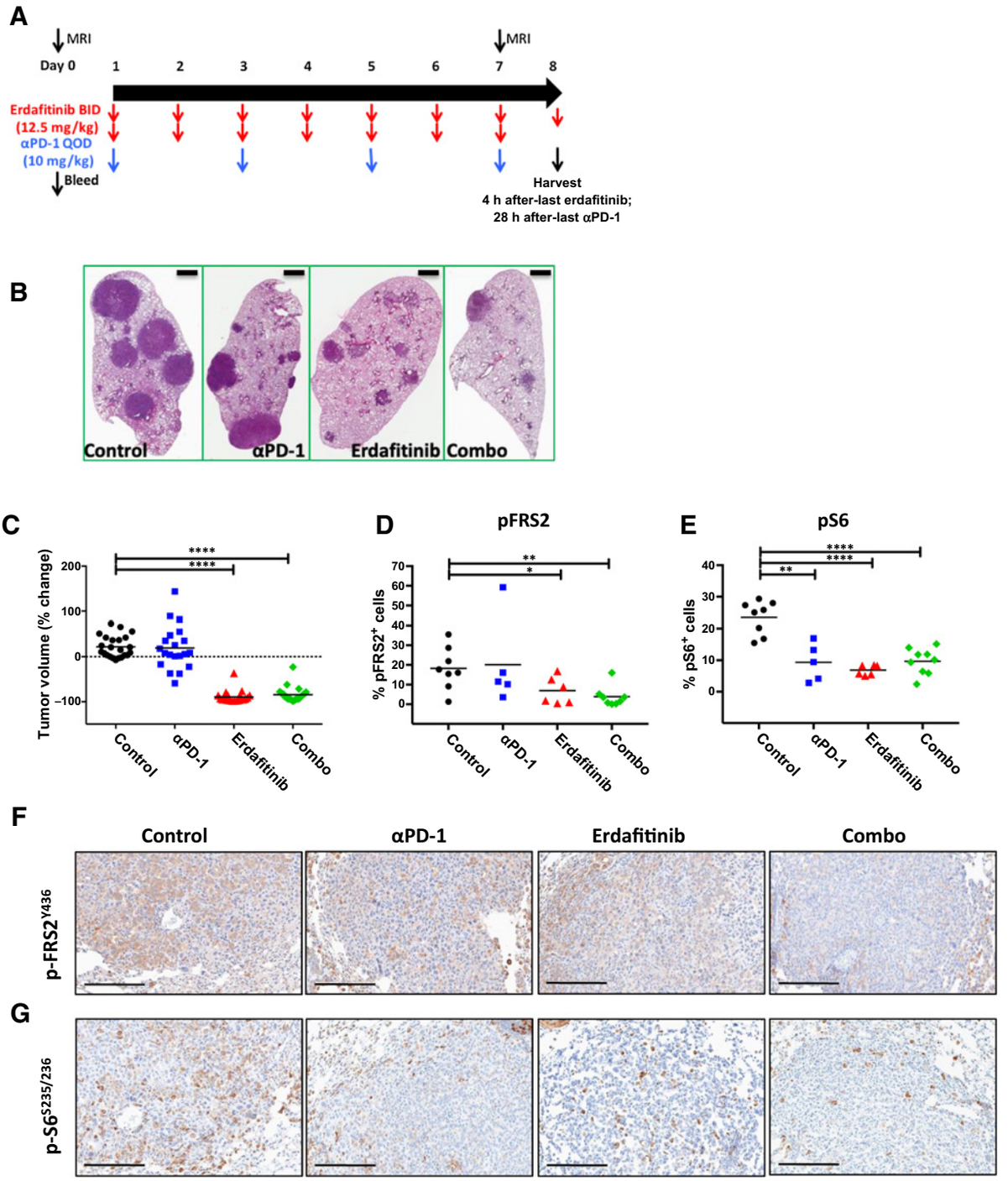

Figure 2.

Inhibition of FGFR signaling in FKNP tumors. **A,** Pharmacodynamic study design. Pretreatment blood was collected a day before the start of the treatment. Treated mice were harvested for tumors and blood on day 8 for IHC, flow cytometry, and TCR sequencing analyses. Control $n = 23$, anti–PD-1 $n = 20$, erdafitinib $n = 21$, and combination $n = 24$. BID, every day; h, hours; QOD, every other day. **B,** Representative H&E sections of tumor-bearing lungs at day 8 of treatment for each group. Scale bar, 1 mm. **C,** Changes in percentage of tumor volume of individual mice in each treatment group after a week of treatment, quantified from MRI. ****, $P < 0.0001$, one-way ANOVA. Changes in expression of pFRS2 (**D**) and pS6 (**E**) in treatment groups were quantified using FFPE lung sections. *, $P < 0.05$; **, $P < 0.01$; ****, $P < 0.0001$, Welch t test. Representative IHC images for pFRS2 (**F**) and pS6 (**G**). Scale bar, 50 μm.

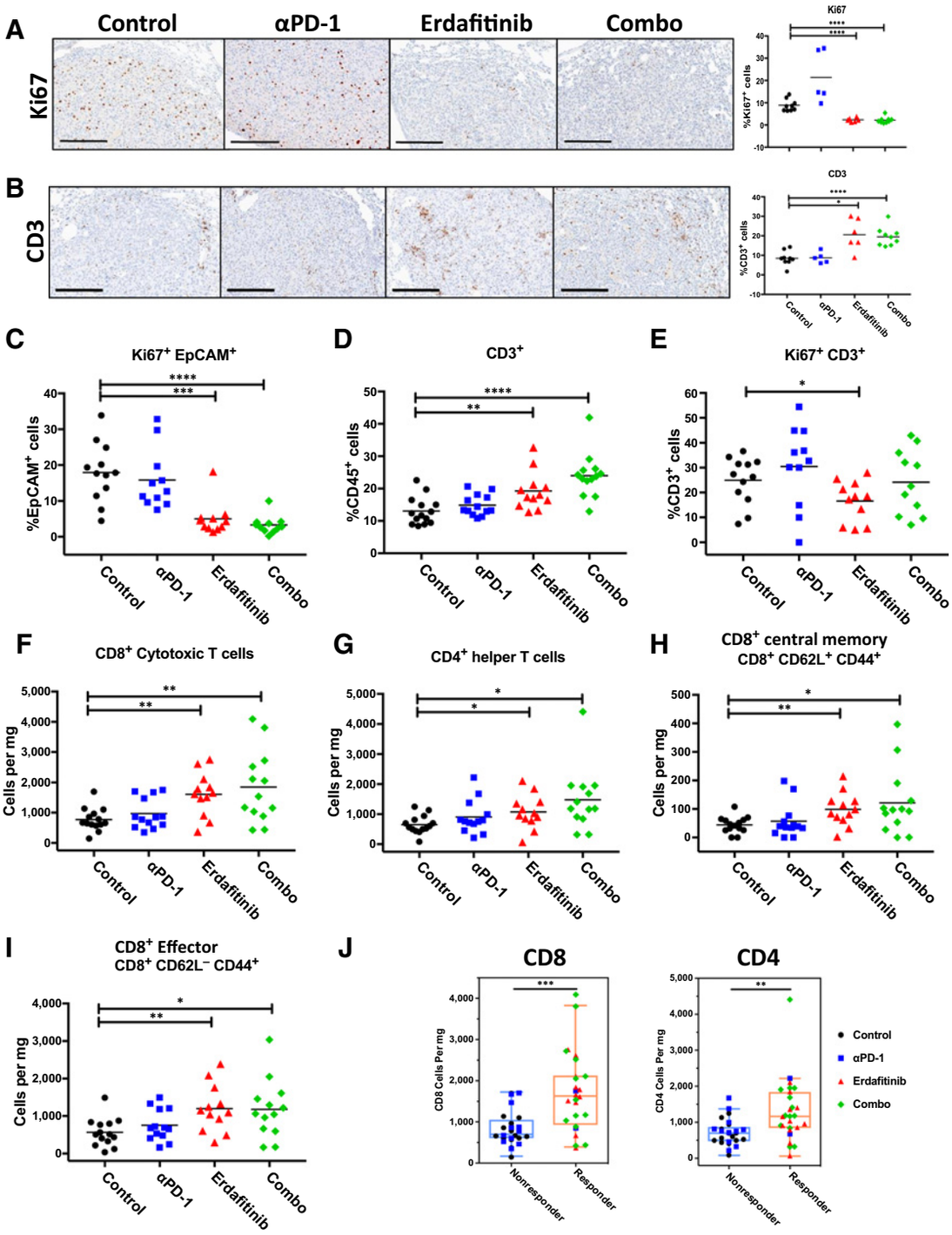

Figure 3.

Effects of erdafitinib and anti–PD-1 on T-cell infiltration and proliferation in FKNP tumors. Changes in immune cell infiltration and proliferation in FKNP tumor-bearing lungs at day 8 of treatment were analyzed. **A** and **B,** Representative IHC images (left) and quantified changes (right) by treatment are shown for Ki67$^+$ (**A**) and CD3$^+$ (**B**). Control $n = 9$, anti–PD-1 $n = 5$, erdafitinib $n = 6$, and combination $n = 9$. **C–J,** Flow cytometry analyses are shown for proliferative epithelial cells (EpCAM$^+$Ki67$^+$; **C**), T cells (CD3$^+$; **D**), proliferative T cells (CD3$^+$Ki67$^+$; **E**), CD8$^+$ cytotoxic T cells (CD8$^+$; **F**), CD4$^+$ helper T cells (CD4$^+$; **G**), CD8$^+$ central memory (CD8$^+$CD62L$^+$CD44$^+$; **H**), and CD8$^+$ effectors (CD8$^+$CD62L$^-$CD44$^+$; **I**). Control $n = 14$, anti–PD-1 $n = 13$, erdafitinib $n = 12$, and combination $n = 14$. For **A–I**: *, $P < 0.05$; **, $P < 0.01$; ***, $P < 0.001$; ****, $P < 0.0001$, Welch t test. **J,** Changes in infiltrating CD8$^+$ and CD4$^+$ cells are stratified by tumor response. Boxplots show minimum value, 25th percentile, median, 75th percentile, and maximum values. Responders: >30% tumor regression. **, $P = 0.0012$; ***, $P = 0.0001$, two-tailed Wilcoxon rank sum test.

with antitumor responses (Fig. 3J). Changes in tumor-infiltrating lymphocytes (TIL) in the combination group were accompanied by a trend toward increased abundance of NK and B cells in the TME (Supplementary Fig. S4D–S4G). Overall, anti–PD-1 treatment enhanced proliferation of T and NK cells, such that anti–PD-1– and combination-treated tumors exhibited higher proportions of $Ki67^+$ T cells and NK cells relative to the control and erdafinitib-treated groups, respectively, although the differences did not reach statistical significance (Fig. 3E; Supplementary Fig. S4K–S4M).

The fraction of infiltrating TAMs ($CD11c^+CD11b^-$) was decreased in combination-treated tumors compared with erdafitinib or anti–PD-1 monotherapy groups (Fig. 4A). Decreased proliferating TAMs were observed in both erdafitinib and combination groups (Fig. 4B). Erdafitinib-treated tumors exhibited a significant reduction in Tregs ($Foxp3^+CD25^+CD4^+$ cells) compared with the control group (Fig. 4C). Although erdafitinib treatment alone or in combination with anti–PD-1 did not significantly affect single exhaustion marker (PD-1, TIM-3, or LAG-3) expression on $CD8^+$ or $CD4^+$ T cells (Supplementary Fig. S5A and S5B), it did lead to a trend in the reduction of double exhaustion marker–positive T cells ($PD\text{-}1^+TIM\text{-}3^+$; Supplementary Fig. S5C and S5D) and a significant reduction in triple exhaustion marker–positive ($PD\text{-}1^+Tim3^+Lag3^+$) T cells (Fig. 4D and E), which are considered terminally exhausted T cells (33). Tumors that responded (>30% tumor regression) to erdafitinib monotherapy or in combination with anti–PD-1 therapy showed higher frequency of NK cells and lower frequency of TAMs (Fig. 4F). To determine whether erdafitinib directly affected immune cells, we tested treatment effects on the viability of human normal PBMCs (both resting or *ex vivo* stimulated with anti-CD3; Supplementary Fig. S6A). T-cell viability remained constant with increasing concentrations of erdafitinib at multiple time points following treatment (days 2 and 6), suggesting that erdafitinib does not directly affect immune cell viability (Supplementary Fig. S6A). We also tested whether erdafitinib affected the activity of anti–PD-1 in two *in vitro* assays that measured T-cell function, a mixed lymphocyte reaction (MLR) and a CMV recall assay (Supplementary Fig. S6B and S6C). In both assays, combination erdafitinib with anti–PD-1 caused a similar increase in IFNγ secretion as anti–PD-1 treatment alone.

Together, these results suggested an indirect effect of erdafitinib on immune cells in the FNKP model through a tumor-intrinsic mechanism. Erdafitinib-treated tumors exhibited higher T-cell infiltration and a reduction in immunosuppressive populations, including Tregs and terminally exhausted T cells. Anti–PD-1 in combination with erdafinitib led to additional changes in the immune TME, including decreased infiltration of immunosuppressive TAMs, increased NK and B cell abundance, and a higher proliferative, activated state of T and NK cells relative to erdafitinib alone.

Erdafitinib inhibits PD-L1 expression in tumor cells

FGFR exerts its activity primarily through the MAPK, TOR/AKT, and JAK/STAT signaling pathways (34), which are also involved in the regulation of PD-L1 and PD-L2 expression (35). We, therefore, reasoned that erdafitinib could have an impact on PD-L1 expression in the FKNP model. Consistent with this hypothesis, a significant decrease in the expression of PD-L1, but not PD-L2, was observed in tumor cells upon treatment with erdafitinib (Fig. 5A–C; Supplementary Fig. S4H and S4I). No effect was observed on PD-L1 expression on TAMs (Fig. 5D), suggesting that this is a specific effect mediated through inhibition of FGFR in tumor cells. Further supporting this idea, elevated tumor PD-L1 expression in the FGFR-insensitive $KRAS^{G12C}$ -driven lung adenocarcinoma model was unchanged upon treatment with erdafitinib (Supplementary Fig. S3C).

To investigate the underlying mechanism of reduced PD-L1 expression upon FGFR inhibitor treatment, we first showed that human lung cancers that harbor *FGFR* and *KRAS* alterations showed a broad range of PD-L1 expression, as assessed by IHC analysis (Fig. 5E and F). We then determined that treatment with erdafitinib (and other FGFR inhibitors such as BGJ398 and AZD4547) caused a dose-dependent decrease in IFNγ-induced PD-L1 expression in the *FGFR2*-amplified Kato III cell line (Supplementary Fig. S7A), but not in the *KRAS*-mutant cancer cell line H441 (Supplementary Fig. S7B). In Kato lll, erdafitinib-dependent modulation of PD-L1 expression correlated with blockade of FGFR signaling, as demonstrated by decreases in pFGFR, pS6, pERK, and pSTAT3 (Fig. 5H; Supplementary Fig. S7C). Individual pathway blockade using inhibitors of mTOR, MEK1/2, JAK1/2, or STAT3/5 did not recapitulate this effect (Supplementary Fig. S7D and S7E), suggesting that simultaneous blockade of several FGFR downstream pathways may be required to achieve the full magnitude of PD-L1 expression modulation.

Erdafitinib monotherapy or in combination with anti–PD-1 alters the T-cell repertoire

We hypothesized that tumor cell death induced directly by erdafitinib can lead to priming of self-reactive T cells and selection of novel tumor-specific T lymphocytes. We performed next-generation immunosequencing using genomic DNA isolated from blood and tumor samples from animals in the different treatment groups to characterize the complementarity-determining region 3 (CDR3) of TCRβ chains. Early changes (8 days after treatment) in the frequency of T cells within the tumor and their clonality were correlated with tumor responses and flow phenotypic profiles. In tumors, both T-cell fraction and clonality were increased after anti–PD-1 treatment compared with the control group (Fig. 6A). Treatment with erdafitinib resulted in decreased clonality, reflective of a T-cell population with a more balanced clone frequency distribution and, therefore, less clonal. The decreased clonality observed in erdafitinib-treated tumors may reflect priming of immune responses through exposure of antigen-presenting cells (APC) to the tumor antigen repertoire as a result of tumor cell apoptosis directly induced by treatment. Combination with anti–PD-1 resulted in a significant increase in both T-cell fraction and clonality compared with erdafitinib treatment alone (Fig. 6A), consistent with anti–PD-1 treatment driving expansion of tumor-specific T-cell clones in the TME (36). A higher T-cell fraction (Fig. 6B) together with lower clonality (Fig. 6C) was observed in tumors that were responsive to erdafinitib and to a greater extent with the combination treatment (Fig. 6B). The clonality readout seemed to be inversely correlated with antitumor responses (Fig. 6C), suggesting that the increased clonality observed in the anti–PD-1 group was not productive.

Longitudinal analysis of the circulating T-cell repertoire revealed that clones that expanded in the blood were also present in the tumor (Fig. 6D), with the anti–PD-1 and anti–PD-1/erdafitinib treatment groups trending toward higher numbers of these expanding clones. In the anti–PD-1– and combination-

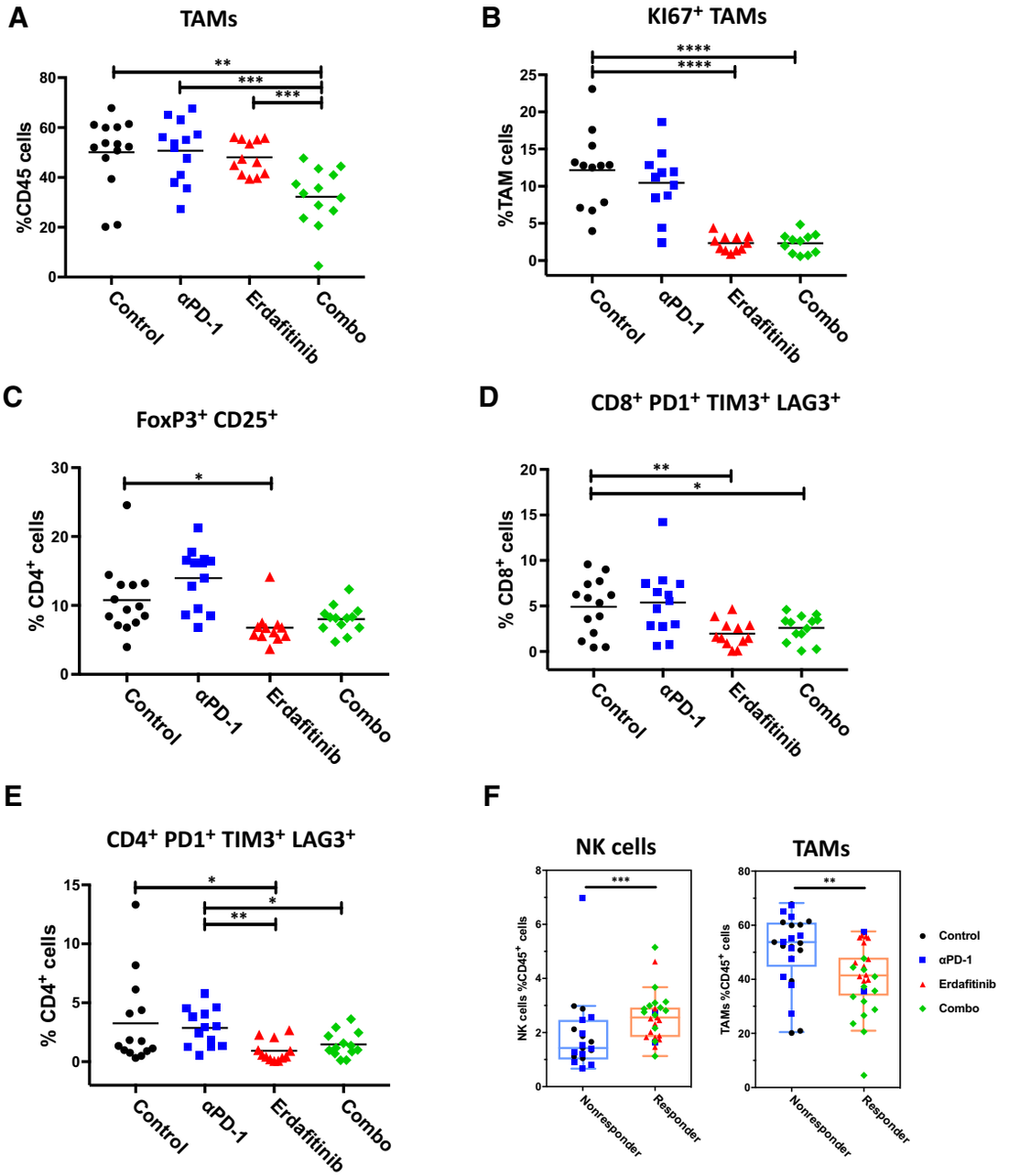

Figure 4.

Changes in immune cell infiltration and T-cell exhaustion with treatment. Flow cytometry analyses of TILs in FKNP tumor–bearing lungs at day 8 of treatment. Changes with treatment in TAMs ($CD11c^+CD11b^-$; **A**) and proliferative TAMs ($CD11c^+CD11b^-Ki67^+$; **B**). **, $P < 0.01$; ***, $P < 0.001$; ****, $P < 0.0001$, Welch t test. **C,** Changes with treatment in Tregs ($CD4^+Foxp3^+CD25^+$). Changes with treatment in triple-positive exhaustion markers in $CD8^+$ ($CD8^+PD\text{-}1^+TIM3^+LAG3^+$; **D**) and $CD4^+$ ($CD4^+PD\text{-}1^+$ $TIM3^+LAG3^+$; **E**) T cells. *, $P < 0.05$; **, $P < 0.01$, Welch t test. **F,** Association of abundance of NK cells and TAMs with tumor response. Boxplots show minimum value, 25th percentile, median, 75th percentile, and maximum values. Responders: >30% tumor regression. **, $P < 0.001$; ***, $P < 0.0005$, two-tailed Wilcoxon rank sum test.

treated tumors, clones that had low pretreatment frequency accounted for about half of the total number of expanded clones, suggesting that anti–PD-1 treatment results in the expansion of both existing and previously undetected clones. Erdafitinib predominantly caused expansion of clones that were undetectable (below detection limit) at baseline, consistent with the hypothesis that erdafitinib induces priming of previously undetected clones (Fig. 6E). Unsupervised clustering analysis of high-frequency tumor clones (at a frequency of 1% of the repertoire or greater) revealed that the T-cell repertoire of

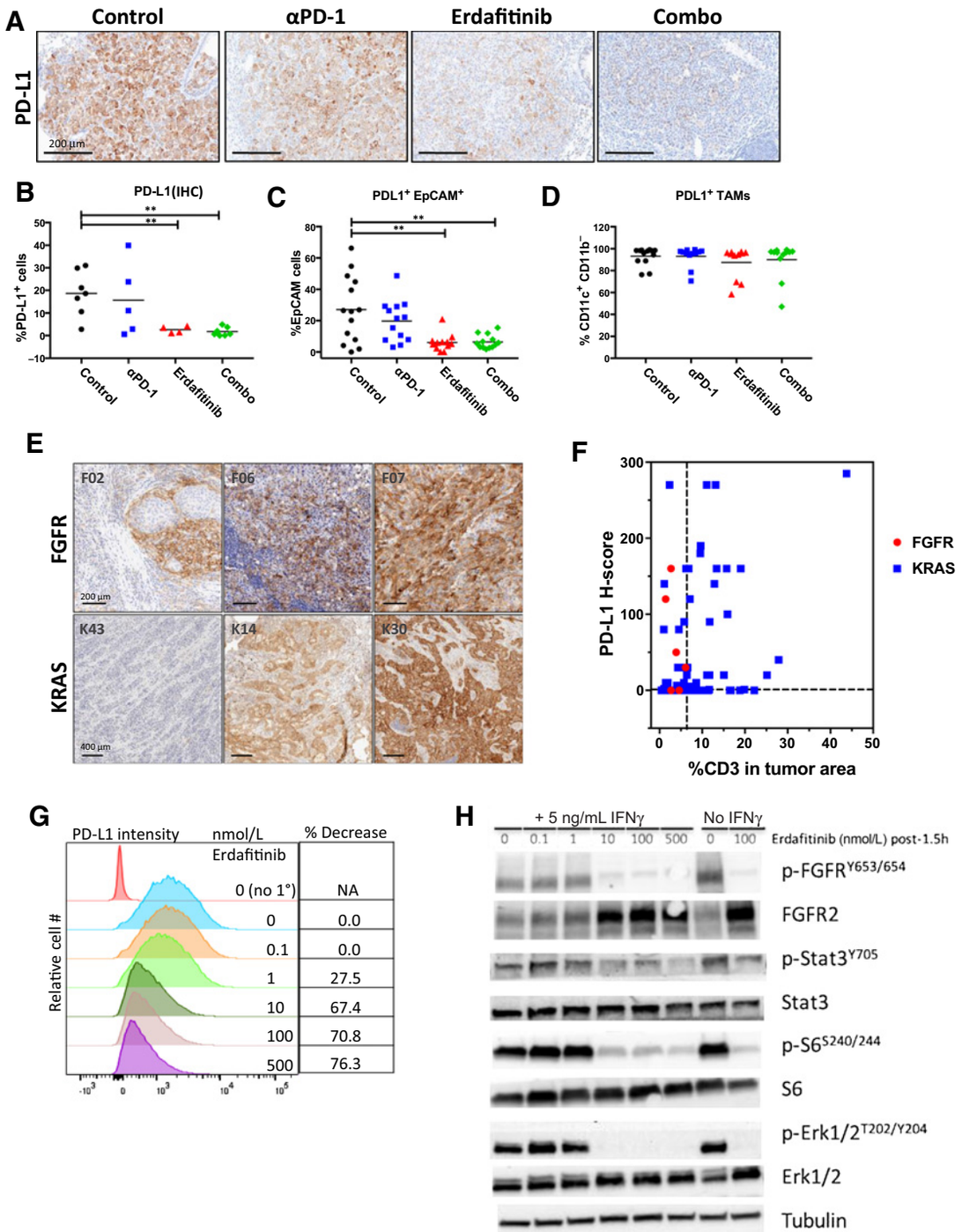

Figure 5.

Erdafitinib inhibits PD-L1 expression. Changes in PD-L1 expression in FKNP tumor–bearing lungs at day 8 of treatment were analyzed. Representative IHC images by treatment (**A**) and quantified changes by treatment (**B**). Scale bar, 200 μm. Flow cytometry showing the frequency of PD-L1^{+}EpCAM^{+} cells (**C**) and PD-L1^{+}TAMs (**D**). PD-L1 expression was assessed in archived human lung cancer patient samples with *FGFR* alterations or *KRAS* mutations by IHC (**E**), with images representative of a wide range of PD-L1 expression (scale bar, 200 μm for FGFR and 400 μm for KRAS), and PD-L1 H-score (**F**), plotted vs. percentage of CD3 positivity per sample for patients with FGFR ($n = 6$) or KRAS ($n = 83$) alterations. Kato III cells (*FGFR2*-amplified human gastric cancer model) were treated with 0 to 500 nmol/L erdafitinib as indicated in the presence of IFNγ (5 ng/mL), and percentage decrease in PD-L1 expression relative to vehicle control–treated cells was assessed 24 hours later by flow cytometry (**G**) and FGFR signaling (**H**) evaluated 1.5 hours following treatment by Western blot. Samples cultured in the presence or absence of 5 ng/mL IFNγ included; tubulin probed as protein loading control. h, hours; NA, not applicable. **, $P < 0.01$; Welch *t* test.

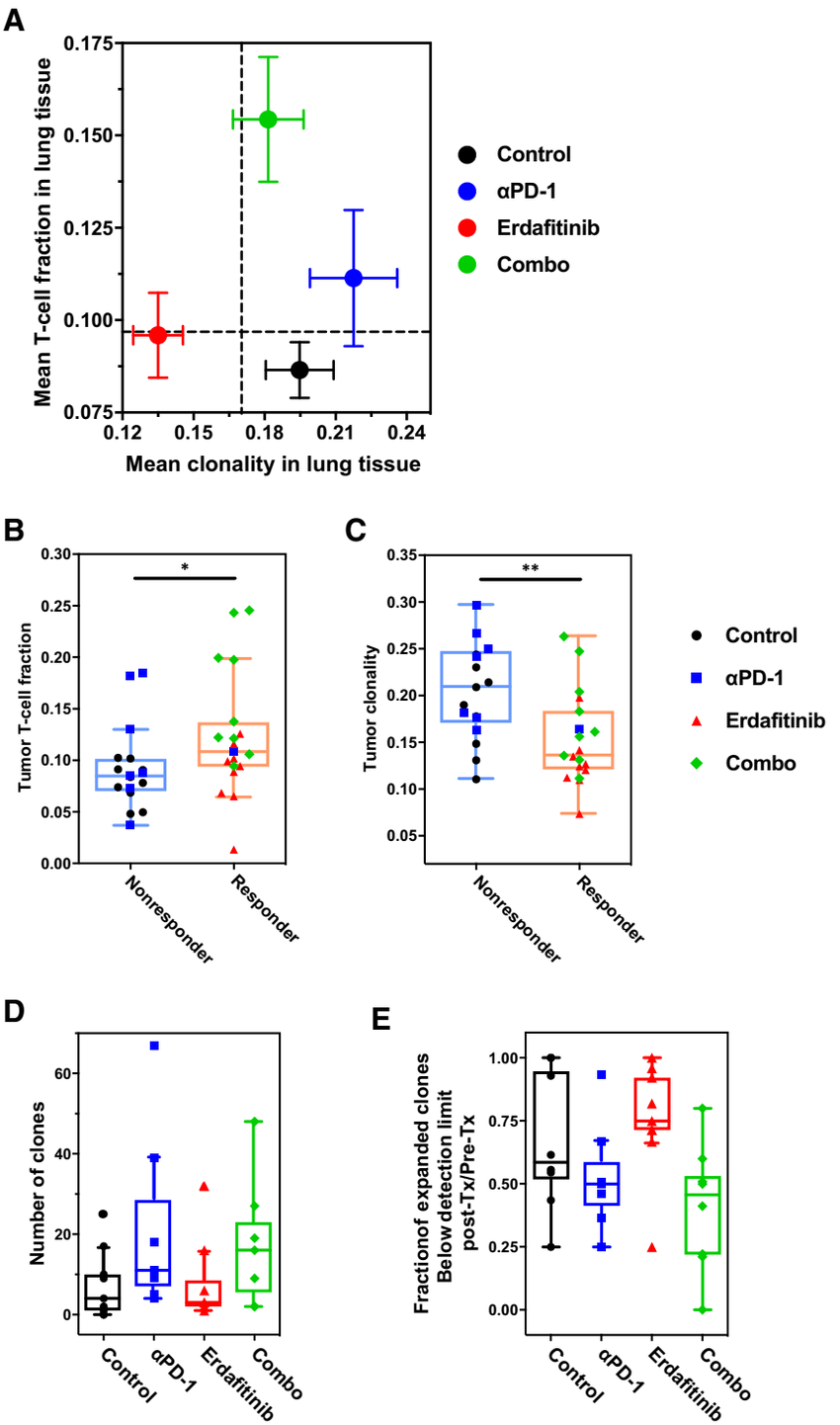

Figure 6.

Erdafitinib and anti–PD-1 treatment alter T-cell infiltration and clonality. **A,** T-cell infiltration and T-cell clonality were determined by TCRβ immunosequencing of FKNP lung tumors harvested at day 8 posttreatment start. Mean with SEM is shown for each group. Control $n = 10$, anti–PD-1 $n = 8$, erdafitinib $n = 9$, and combination treated $n = 9$. T-cell fraction (**B**) and clonality (**C**) in lung tumors in responders (>30% decrease in tumor volume) and nonresponders. **D,** Number of expanding T-cell clones in peripheral blood at day 8 compared with baseline, which are also found in tumors, are depicted for each treatment group ($P = 0.139$, Mann–Whitney). **E,** Fraction of expanded T-cell clones in peripheral blood at day 8 that were below detection at baseline are shown for individual treatment groups (*post hoc* $P = 0.041$). Boxplots show minimum value, 25th percentile, median, 75th percentile, and maximum values. Tx, treatment. *, $P < 0.05$; **, $P < 0.001$, two-tailed Wilcoxon rank sum test.

individual mice was private, with few clones shared between mice within or across treatment groups (Supplementary Fig. S8).

Discussion

Targeted therapies can induce deep responses in patients with NSCLC by blocking actionable mutations, such as EGFR, that are essential for tumor cell growth and progression (37). In contrast, immunotherapy agents, such as those targeting the PD-1 pathway, have demonstrated clinical activity in patients by reactivating preexisting antitumor immune responses (38) but only benefit a subset of patients. Interestingly, driver pathway segments in NSCLC such as EGFR, ALK, and KRAS show limited benefit with immunotherapy, suggesting that these oncogenes

induce changes in the TME, leading to escape from tumor immunosurveillance (39). As a result, significant efforts are ongoing to identify and develop combinations that could harness the nonoverlapping mechanisms of action of targeted agents and immunotherapy to broaden and increase the durability of clinical responses. Key to this concept is the ability of targeted therapies to induce immunogenic cell death that enhances tumor antigen presentation to T cells (40), whose functionality can be enhanced by the immune-activating potential of checkpoint inhibitors. In this study, we demonstrated that the combination of erdafitinib, a pan-FGFR small-molecule inhibitor (9), and PD-1 blockade led to inhibition of tumor growth and a survival advantage in FKNP mice, an *FGFR2*-driven autochthonous lung cancer GEMM (7). We provide evidence that the synergistic antitumor effect of this combination was dependent on erdafitinib-induced tumor cell killing, *de novo* priming, and enhancement of antitumor T-cell responses via PD-1 blockade.

Consistent with the previously described sensitivity of the FKNP model to FGFR inhibition (7), erdafitinib blocked FGFR signaling and exhibited potent antitumor efficacy. In contrast, this model was refractory to PD-1 blockade despite displaying high PD-L1 expression on both tumor and infiltrating immune cells. The combined inhibition of both FGFR and PD-1 led to similar initial tumor growth control compared with erdafitinib monotherapy but resulted in enhanced survival relative to the monotherapy-treated groups. Our data suggest that erdafitinib treatment leads to indirect enhancement of both adaptive and innate immunity *in vivo*, although it does not directly affect immune cell viability and responses *in vitro*. These effects were not observed in a $KRAS^{G12C}$-mutant GEMM that is insensitive to FGFR inhibition, indicating that the *in vivo* immune changes mediated by erdafitinib may be initiated as a consequence of tumor cell killing.

Erdafitinib treatment drove infiltration of both $CD4^+$ helper and $CD8^+$ effector T cells, while reducing the numbers of Tregs and terminally exhausted $CD4^+$ and $CD8^+$ T cells. This effect was dependent on tumor cell killing, because erdafitinib treatment in the nonresponsive $KRAS^{G12C}$-mutant model did not lead to a similar effect. Consistent with these data, it has been shown that direct killing of tumor cells with chemotherapy or targeted agents such as BRAF and MEK inhibitors causes immunogenic cell death and enhances immunogenicity by driving reexpression of tumor antigens and T-cell infiltration, ultimately leading to increased sensitivity to checkpoint blockade (41, 42). Activation of the FGFR3 pathway is associated with non-T cell–inflamed tumors (29) resistant to checkpoint blockade, suggesting that inhibition of the FGFR pathway may be used as a means to elicit T-cell infiltration. Although erdafitinib induced changes in the TME consistent with an enhanced antitumor immune phenotype, this treatment alone did not result in survival benefit. In contrast, similar effects on infiltrating T cells in the anti–PD-1/erdafitinib combination group resulted in enhanced survival, suggesting that additional mechanisms drive more productive and durable immune responses with the combination in this model.

We hypothesized that the survival benefit observed in the combination-treated mice could result from anti–PD-1–mediated enhancement of antitumor T-cell responses primed by erdafitinib-induced cell killing. We proposed that these effects would be reflected in changes in the T-cell repertoire, which could be assayed by TCR sequencing of peripheral blood and tumors. In line with this hypothesis, treatment with erdafitinib resulted in a broader T-cell repertoire, consistent with priming of T-cell responses as a result of APC exposure to the diverse tumor antigen pool released following cell killing (43). Analysis of the peripheral T-cell repertoire supported this hypothesis by showing that erdafitinib-treated mice had higher numbers of previously undetected clones following treatment compared with baseline than other groups. Anti–PD-1 treatment resulted in increased clonality, reflecting a focusing of preexisting T-cell responses, as previously reported in both preclinical and clinical settings (36, 44). Our observation that groups treated with anti–PD-1, either as monotherapy or in combination with erdafitinib, had increased numbers of tumor-specific clones that were expanded in the periphery is consistent with results in the clinic, where tumors that exhibited a pathologic response to neoadjuvant anti–PD-1 treatment had higher frequency of T-cell clones that were shared between the tumor and periphery (45). The lack of monotherapy activity with anti–PD-1 in the FKNP model suggests that activation by anti–PD-1 of T-cell clones present at baseline in tumors may not be sufficient to drive productive antitumor responses. The combination of erdafitinib and anti–PD-1 led to an increase in T-cell clonality relative to erdafitinib monotherapy, suggestive of expansion of tumor-specific T-cell clones induced by erdafitinib. Therefore, our results support a model where erdafitinib primes the immune system by diversifying the T-cell repertoire, and PD-1 blockade drives clonal expansion and reinvigorates $CD8^+$ TILs in the TME.

Erdafitinib and anti–PD-1 combination treatment induced unique changes in the TME in both lymphoid and myeloid populations, consistent with an antitumor phenotype. An orchestrated engagement of various immune cell populations, including decreased numbers of immunosuppressive TAMs, a trend toward increased DC activation, and NK and B cell infiltration, may be essential in the combination-treated mice to trigger deeper antitumor responses, especially in the context of cancers with limited tumor antigens, as represented by GEMM models (46). The shift in the microenvironment of combination-treated tumors toward a more productive inflammatory milieu likely supports and/or enhances antitumor immune responses (47). Limited studies to date have explored the effect of FGFR pathway modulation on the immune subsets mentioned above. For example, activation of FGFR1 has been shown to induce macrophage recruitment in tumors via CX3CL1 induction (48). Inhibition of FGFR has been reported to decrease myeloid-derived suppressor cells (MDSC) and enhance T-cell infiltration in 4T1 breast tumors, although these effects could be due to the additional targeting of CSF1R (49–51). Therefore, the mechanisms through which FGFR inhibition alone or in combination with PD-1 blockade alters specific immune subsets in the TME such as TAMs, DCs, and NK and B cells remain to be explored further.

Here, we showed that in human lung tumors, FGFR alterations were correlated with low T-cell infiltration independent of PD-L1 expression. Consistently, the TME in FKNP mice was characterized by high PD-L1 expression in both tumor and immune cells and by low T-cell infiltration. Treatment with erdafitinib led to PD-L1 downregulation in FGFR-expressing tumor cells (*in vivo* and *in vitro*), but not in macrophages. Our *in vitro* results show that erdafitinib reduced IFNγ-induced PD-L1 expression, suggesting that this could be the mechanism that leads to reduced PD-L1 in FKNP tumors. These data, together with the observation that erdafitinib had no effect on

PD-L1 expression in the $KRAS^{G12C}$ model, indicated that the effect on PD-L1 was specifically mediated via FGFR blockade on tumor cells. Downregulation of PD-L1 in tumor cells was consistent with a shift toward a less immunosuppressive TME that was more permissive to T-cell infiltration, although these changes did not result in survival benefit perhaps due, in part, to the fact that PD-L1 expression on either tumor cells or host immune cells can lead to tumor escape from immune control (52). Despite the high PD-L1 expression, treatment with anti–PD-1 monotherapy did not result in significant T-cell infiltration, tumor control, or survival benefit, suggesting that other mechanisms of resistance may be at play. Primary resistance to PD-1 blockade may be a consequence of FGFR alterations on tumor cells driving an immune-suppressive TME, as it has been shown for FGFR3-mutant bladder cancer (29). Consistently, combination with erdafitinib overcame the immunosuppressive environment, allowing for T-cell infiltration and specific antitumor responses that led to a significant survival advantage. The enhanced survival benefit with the combination could also be attributed to a more complete shutdown of the PD-1/PD-L1 axis via erdafitinib-driven inhibition of PD-L1 on tumor cells and anti–PD-1–mediated blockade of PD-L1 on host immune cells.

In summary, our data uncovered key aspects of the mechanism underlying the superior antitumor efficacy resulting from the combination of erdafitinib and anti–PD-1 through both tumor-intrinsic and immune-modulatory effects. We showed that erdafitinib treatment could drive T-cell infiltration and cause *de novo* priming and broadening of the T-cell repertoire likely via an indirect mechanism that depends on tumor cell killing. The addition of PD-1 blockade to erdafitinib treatment led to focusing of the T-cell repertoire through expansion of specific T-cell clones that were likely critical to induce productive antitumor immune responses. These data provide a rationale for the clinical evaluation of erdafitinib in combination with PD-1/PD-L1 blocking agents in patients with FGFR-altered tumors, which have poor T-cell infiltration and are normally refractory to PD-1 blockade.

Disclosure of Potential Conflicts of Interest

E. Zudaire has ownership interest (including stock, patents, etc.) in Johnson & Johnson. C. Ferrante has ownership interest (including stock, patents, etc.) in Johnson & Johnson. J.M. English is Chief Scientific Officer at TILOS Therapeutics and Vice President and Head of Discovery, Immuno-Oncology, at EMD Serono. A.H. Beck has ownership interest (including stock, patents, etc.) in PathAI. J.A. Rytlewski is Senior Computational Biologist at and has ownership interest (including stock, patents, etc.) in Adaptive Biotechnologies. C. Sanders has ownership interest (including stock, patents, etc.) in Adaptive Biotechnologies. K. Packman has ownership interest (including stock, patents, etc.) in Johnson & Johnson. P.A. Janne reports receiving commercial research grants from Astellas, AstraZeneca, Boehringer Ingelheim, Daiichi Sankyo, Takeda Oncology, and Eli Lilly, has ownership interest (including stock, patents, etc.) in Gatekeeper Pharmaceuticals and LOXO Oncology, is a consultant/advisory board member for AstraZeneca, Boehringer Ingelheim, Voronoi, SFJ Pharmaceuticals, Biocartis, ACEA Biosciences, Araxes, Ignyta, Pfizer, Genentech/Roche, Merrimack Pharmaceuticals, Chugai Pharmaceuticals, Eli Lilly, Novartis, Daiichi Sankyo, and Takeda Oncology, and has provided expert testimony for LabCorp. K.-K. Wong reports receiving a commercial research grant from Janssen Pharmaceuticals, MedImmune, Novartis, Pfizer, Merck, Takeda, and Mirati and has ownership interest (including stock, patents, etc.) in G1 Therapeutics. R.I. Verona has ownership interest (including stock, patents, etc.) in Johnson & Johnson. M.V. Lorenzi has ownership interest (including stock, patents, etc.) in Johnson & Johnson. No potential conflicts of interest were disclosed by the other authors.

Authors' Contributions

Conception and design: S. Palakurthi, M. Kuraguchi, S.J. Zacharek, E. Zudaire, C. Ferrante, S. Laquerre, M.A. Bittinger, K. Packman, K.-K. Wong, R.I. Verona, M.V. Lorenzi

Development of methodology: S. Palakurthi, M. Kuraguchi, S.J. Zacharek, K. DePeaux, C. Ferrante, M.A. Bittinger

Acquisition of data (provided animals, acquired and managed patients, provided facilities, etc.): S. Palakurthi, M. Kuraguchi, S.J. Zacharek, W. Huang, D.M. Bonal, J. Liu, A. Dhaneshwar, K. DePeaux, M.R. Gowaski, D. Bailey, S.N. Regan, E. Ivanova, C. Ferrante, P.A. Janne, K.-K. Wong

Analysis and interpretation of data (e.g., statistical analysis, biostatistics, computational analysis): S. Palakurthi, M. Kuraguchi, S.J. Zacharek, E. Zudaire, W. Huang, A. Dhaneshwar, K. DePeaux, M.R. Gowaski, D. Bailey, E. Ivanova, C. Ferrante, A. Khosla, A.H. Beck, J.A. Rytlewski, C. Sanders, M.A. Bittinger, C. Moy, K.-K. Wong, R.I. Verona, M.V. Lorenzi

Writing, review, and/or revision of the manuscript: S. Palakurthi, M. Kuraguchi, S.J. Zacharek, E. Zudaire, K. DePeaux, M.R. Gowaski, E. Ivanova, C. Ferrante, A.H. Beck, J.A. Rytlewski, S. Laquerre, P.T. Kirschmeier, K. Packman, P.A. Janne, R.I. Verona, M.V. Lorenzi

Administrative, technical, or material support (i.e., reporting or organizing data, constructing databases): M. Kuraguchi, S.J. Zacharek, W. Huang, D.M. Bonal, A. Dhaneshwar, M.R. Gowaski, C. Ferrante, A.H. Beck, K. Packman, R.I. Verona

Study supervision: S. Palakurthi, M. Kuraguchi, S.J. Zacharek, E. Zudaire, C. Ferrante, J.M. English, P.T. Kirschmeier, R.I. Verona, M.V. Lorenzi

Acknowledgments

The authors thank Dana-Farber Cancer Institute Hematologic Neoplasia Flow Cytometry Core for help with flow cytometry, Harvard Medical School Rodent Pathology Core and Roderick Bronson for tissue processing, Brigham and Women's Pathology Core and Mei Zhang for help with tissue staining, and Lurie Family Imaging Center with mouse MRI.

The costs of publication of this article were defrayed in part by the payment of page charges. This article must therefore be hereby marked *advertisement* in accordance with 18 U.S.C. Section 1734 solely to indicate this fact.

Received August 30, 2018; revised January 30, 2019; accepted July 17, 2019; published first July 22, 2019.

References

1. Wong MCS, Lao XQ, Ho KF, Goggins WB, Tse SLA. Incidence and mortality of lung cancer: global trends and association with socioeconomic status. Sci Rep 2017;7:14300.
2. Wesche J, Haglund K, Haugsten EM. Fibroblast growth factors and their receptors in cancer. Biochem J 2011;437:199–213.
3. Turner N, Grose R. Fibroblast growth factor signalling: from development to cancer. Nat Rev Cancer 2010;10:116–29.
4. Lorenzi MV, Horii Y, Yamanaka R, Sakaguchi K, Miki T. FRAG1, a gene that potently activates fibroblast growth factor receptor by C-terminal fusion through chromosomal rearrangement. Proc Natl Acad Sci U S A 1996;93:8956–61.
5. Weiss J, Sos ML, Seidel D, Peifer M, Zander T, Heuckmann JM, et al. Frequent and focal FGFR1 amplification associates with therapeutically tractable FGFR1 dependency in squamous cell lung cancer. Sci Transl Med 2010;2:62ra93.
6. Cancer Genome Atlas Research N. Comprehensive genomic characterization of squamous cell lung cancers. Nature 2012;489:519–25.

7. Tchaicha JH, Akbay EA, Altabef A, Mikse OR, Kikuchi E, Rhee K, et al. Kinase domain activation of FGFR2 yields high-grade lung adenocarcinoma sensitive to a Pan-FGFR inhibitor in a mouse model of NSCLC. Cancer Res 2014;74:4676–84.
8. Karkera JD, Cardona GM, Bell K, Gaffney D, Portale JC, Santiago-Walker A, et al. Oncogenic characterization and pharmacologic sensitivity of activating fibroblast growth factor receptor (FGFR) genetic alterations to the selective FGFR inhibitor erdafitinib. Mol Cancer Ther 2017;16: 1717–26.
9. Perera TPS, Jovcheva E, Mevellec L, Vialard J, De Lange D, Verhulst T, et al. Discovery and pharmacological characterization of JNJ-42756493 (erdafitinib), a functionally selective small-molecule FGFR family inhibitor. Mol Cancer Ther 2017;16:1010–20.
10. Tabernero J, Bahleda R, Dienstmann R, Infante JR, Mita A, Italiano A, et al. Phase I dose-escalation study of JNJ-42756493, an oral pan-fibroblast growth factor receptor inhibitor, in patients with advanced solid tumors. J Clin Oncol 2015;33:3401–8.
11. Soria JC, Italiano A, Cervantes A, Tabernero J, Infante J, Lara PN, et al. Safety and activity of the pan-fibroblast growth factor receptor (FGFR) inhibitor erdafitinib in phase 1 study patients with advanced urothelial carcinoma. Ann Oncol 2016;27(suppl_6):781PD.
12. Spranger S, Bao R, Gajewski TF. Melanoma-intrinsic beta-catenin signalling prevents anti-tumour immunity. Nature 2015;523:231–5.
13. Rizvi NA, Hellmann MD, Snyder A, Kvistborg P, Makarov V, Havel JJ, et al. Cancer immunology. Mutational landscape determines sensitivity to PD-1 blockade in non-small cell lung cancer. Science 2015;348: 124–8.
14. Gainor JF, Shaw AT, Sequist LV, Fu X, Azzoli CG, Piotrowska Z, et al. EGFR mutations and ALK rearrangements are associated with low response rates to PD-1 pathway blockade in non-small cell lung cancer: a retrospective analysis. Clin Cancer Res 2016;22:4585–93.
15. Gettinger S, Politi K. PD-1 axis inhibitors in EGFR- and ALK-driven lung cancer: lost cause? Clin Cancer Res 2016;22:4539–41.
16. Spranger S, Gajewski TF. Impact of oncogenic pathways on evasion of antitumour immune responses. Nat Rev Cancer 2018;18:139–47.
17. McFadden DG, Politi K, Bhutkar A, Chen FK, Song X, Pirun M, et al. Mutational landscape of EGFR-, MYC-, and Kras-driven genetically engineered mouse models of lung adenocarcinoma. Proc Natl Acad Sci U S A 2016;113:E6409–E17.
18. DuPage M, Dooley AL, Jacks T. Conditional mouse lung cancer models using adenoviral or lentiviral delivery of Cre recombinase. Nat Protoc 2009;4:1064–72.
19. Li S, Liu S, Deng J, Akbay EA, Hai J, Ambrogio C, et al. Assessing therapeutic efficacy of MEK inhibition in a KRAS G12C-driven mouse model of lung cancer. Clin Cancer Res 2018;24:4854–64.
20. Cardarella S, Ogino A, Nishino M, Butaney M, Shen J, Lydon C, et al. Clinical, pathologic, and biologic features associated with BRAF mutations in non-small cell lung cancer. Clin Cancer Res 2013;19: 4532–40.
21. Cardarella S, Ortiz TM, Joshi VA, Butaney M, Jackman DM, Kwiatkowski DJ, et al. The introduction of systematic genomic testing for patients with non-small-cell lung cancer. J Thorac Oncol 2012;7: 1767–74.
22. Robins H, Desmarais C, Matthis J, Livingston R, Andriesen J, Reijonen H, et al. Ultra-sensitive detection of rare T cell clones. J Immunol Methods 2012;375:14–9.
23. Robins HS, Campregher PV, Srivastava SK, Wacher A, Turtle CJ, Kahsai O, et al. Comprehensive assessment of T-cell receptor beta-chain diversity in alphabeta T cells. Blood 2009;114:4099–107.
24. Carlson CS, Emerson RO, Sherwood AM, Desmarais C, Chung MW, Parsons JM, et al. Using synthetic templates to design an unbiased multiplex PCR assay. Nat Commun 2013;4:2680.
25. Kirsch I, Vignali M, Robins H. T-cell receptor profiling in cancer. Mol Oncol 2015;9:2063–70.
26. DeWitt WS, Emerson RO, Lindau P, Vignali M, Snyder TM, Desmarais C, et al. Dynamics of the cytotoxic T cell response to a model of acute viral infection. J Virol 2015;89:4517–26.
27. Perera-Bel J, Hutter B, Heining C, Bleckmann A, Frohlich M, Frohling S, et al. From somatic variants towards precision oncology: evidence-driven reporting of treatment options in molecular tumor boards. Genome Med 2018;10:18.
28. Cancer Genome Atlas Research Network. Comprehensive molecular profiling of lung adenocarcinoma. Nature 2014;511:543–50.
29. Sweis RF, Spranger S, Bao R, Paner GP, Stadler WM, Steinberg G, et al. Molecular drivers of the non-T-cell-inflamed tumor microenvironment in urothelial bladder cancer. Cancer Immunol Res 2016;4:563–8.
30. Koyama S, Akbay EA, Li YY, Aref AR, Skoulidis F, Herter-Sprie GS, et al. STK11/LKB1 deficiency promotes neutrophil recruitment and proinflammatory cytokine production to suppress T-cell activity in the lung tumor microenvironment. Cancer Res 2016; 76:999–1008.
31. Turner N, Pearson A, Sharpe R, Lambros M, Geyer F, Lopez-Garcia MA, et al. FGFR1 amplification drives endocrine therapy resistance and is a therapeutic target in breast cancer. Cancer Res 2010;70: 2085–94.
32. Turner N, Lambros MB, Horlings HM, Pearson A, Sharpe R, Natrajan R, et al. Integrative molecular profiling of triple negative breast cancers identifies amplicon drivers and potential therapeutic targets. Oncogene 2010;29:2013–23.
33. Benci JL, Xu B, Qiu Y, Wu TJ, Dada H, Twyman-Saint Victor C, et al. Tumor interferon signaling regulates a multigenic resistance program to immune checkpoint blockade. Cell 2016;167:1540–54.
34. Babina IS, Turner NC. Advances and challenges in targeting FGFR signalling in cancer. Nat Rev Cancer 2017;17:318–32.
35. Chen J, Jiang CC, Jin L, Zhang XD. Regulation of PD-L1: a novel role of pro-survival signalling in cancer. Ann Oncol 2016;27:409–16.
36. Weir GM, Hrytsenko O, Quinton T, Berinstein NL, Stanford MM, Mansour M. Anti-PD-1 increases the clonality and activity of tumor infiltrating antigen specific T cells induced by a potent immune therapy consisting of vaccine and metronomic cyclophosphamide. J Immunother Cancer 2016;4:68.
37. Rotow J, Bivona TG. Understanding and targeting resistance mechanisms in NSCLC. Nat Rev Cancer 2017;17:637–58.
38. Valecha GK, Vennepureddy A, Ibrahim U, Safa F, Samra B, Atallah JP. Anti-PD-1/PD-L1 antibodies in non-small cell lung cancer: the era of immunotherapy. Expert Rev Anticancer Ther 2017;17:47–59.
39. Liu X, Cho WC. Precision medicine in immune checkpoint blockade therapy for non-small cell lung cancer. Clin Transl Med 2017;6:7.
40. Kroemer G, Galluzzi L, Kepp O, Zitvogel L. Immunogenic cell death in cancer therapy. Annu Rev Immunol 2013;31:51–72.
41. Pfirschke C, Engblom C, Rickelt S, Cortez-Retamozo V, Garris C, Pucci F, et al. Immunogenic chemotherapy sensitizes tumors to checkpoint blockade therapy. Immunity 2016;44:343–54.
42. Hughes PE, Caenepeel S, Wu LC. Targeted therapy and checkpoint immunotherapy combinations for the treatment of cancer. Trends Immunol 2016;37:462–76.
43. Rudqvist NP, Pilones KA, Lhuillier C, Wennerberg E, Sidhom JW, Emerson RO, et al. Radiotherapy and CTLA-4 blockade shape the TCR repertoire of tumor-infiltrating T cells. Cancer Immunol Res 2018;6: 139–50.
44. Tumeh PC, Harview CL, Yearley JH, Shintaku IP, Taylor EJ, Robert L, et al. PD-1 blockade induces responses by inhibiting adaptive immune resistance. Nature 2014;515:568–71.
45. Forde PM, Chaft JE, Smith KN, Anagnostou V, Cottrell TR, Hellmann MD, et al. Neoadjuvant PD-1 blockade in resectable lung cancer. N Engl J Med 2018.
46. Moynihan KD, Opel CF, Szeto GL, Tzeng A, Zhu EF, Engreitz JM, et al. Eradication of large established tumors in mice by combination immunotherapy that engages innate and adaptive immune responses. Nat Med 2016;22:1402–10.
47. Luheshi NM, Coates-Ulrichsen J, Harper J, Mullins S, Sulikowski MG, Martin P, et al. Transformation of the tumour microenvironment by a CD40 agonist antibody correlates with improved responses to PD-L1 blockade in a mouse orthotopic pancreatic tumour model. Oncotarget 2016;7:18508–20.
48. Reed JR, Stone MD, Beadnell TC, Ryu Y, Griffin TJ, Schwertfeger KL. Fibroblast growth factor receptor 1 activation in mammary tumor cells promotes macrophage recruitment in a CX3CL1-dependent manner. PLoS One 2012;7:e45877.
49. Liu L, Ye TH, Han YP, Song H, Zhang YK, Xia Y, et al. Reductions in myeloid-derived suppressor cells and lung metastases using AZD4547 treatment of

a metastatic murine breast tumor model. Cell Physiol Biochem 2014;33:633–45.
50. Ye T, Wei X, Yin T, Xia Y, Li D, Shao B, et al. Inhibition of FGFR signaling by PD173074 improves antitumor immunity and impairs breast cancer metastasis. Breast Cancer Res Treat 2014;143:435–46.
51. Katoh M. FGFR inhibitors: Effects on cancer cells, tumor microenvironment and whole-body homeostasis (review). Int J Mol Med 2016;38:3–15.
52. Noguchi T, Ward JP, Gubin MM, Arthur CD, Lee SH, Hundal J, et al. Temporally distinct PD-L1 expression by tumor and host cells contributes to immune escape. Cancer Immunol Res 2017;5:106–17.